

To Appear in the Astrophysical Journal (Main Journal)

X-ray Emission from the Prototypical LINER Galaxy NGC 1052

K. A. Weaver¹

Johns Hopkins University, Department of Physics and Astronomy, Homewood campus,
3400 North Charles Street, Baltimore, MD 21218; kweaver@pha.jhu.edu

A. S. Wilson²

Space Telescope Science Institute, 3700 San Martin Drive, Baltimore, MD 21218;
awilson@stsci.edu

C. Henkel

Max-Planck-Institut für Radioastronomie, Auf dem Hügel 69, D-53121 Bonn, Germany;
p220hen@mpifr-bonn.mpg.de

and

J. A. Braatz

National Radio Astronomy Observatory, P. O. Box 2, Green Bank, WV 24944;
jbraatz@nrao.edu

ABSTRACT

We examine the 0.1 to 10.0 keV X-ray spectrum of the bright nuclear LINER galaxy NGC 1052, one of two elliptical galaxies known to contain a luminous H₂O maser. The observed 2.0 – 10.0 keV spectrum is unusually flat (photon index $\Gamma \sim 0.2$) and best described as intrinsically power-law shaped nuclear flux that is either (1) attenuated by a complex absorber with $\sim 70\%$ of the nuclear flux absorbed by a column density of $N_{\text{H}} \sim 3 \times 10^{23} \text{ cm}^{-2}$ and $\sim 30\%$ absorbed by a column density of $N_{\text{H}} \sim 3 - 5 \times 10^{22} \text{ cm}^{-2}$, or (2) reprocessed, with the nuclear source blocked and the X-rays Compton reflected in our direction by high column density ($\geq 10^{24} \text{ cm}^{-2}$) gas. The moderate equivalent width of the Fe K α line favors the dual absorption model as the most likely scenario. The 0.1 – 2.0 keV spectrum does not resemble the few times 10^6 to 10^7 K thermal

¹Also NASA Goddard Space Flight Center, Greenbelt, MD 20771

²Also Astronomy Department, University of Maryland, College Park, MD 20742; wilson@astro.umd.edu

emission typically found in other elliptical galaxies, but instead is best described as nuclear X-rays leaking through a patchy absorber or scattered in our direction by low-density, ionized gas with the thermal contribution limited to about 15% for solar abundances. The absorption-corrected 2 – 10 keV luminosity of the nuclear source is $L_X \sim 8 \times 10^{41}$ ergs s⁻¹ or $L_X \sim 2 \times 10^{43}$ ergs s⁻¹ for the dual-absorption and Compton-reflection models, respectively. The absorbing and H₂O masing gases appear to be spatially separate in this galaxy.

Subject headings: galaxies: individual (NGC 1052) – galaxies: nuclei – galaxies: Seyfert – X-rays: galaxies – masers

1. Introduction

Water vapor “megamasers” with isotropic luminosities of ~ 20 to $6000 L_{\odot}$ have been detected in eighteen galaxies to date (Braatz, Wilson & Henkel 1996; Greenhill et al. 1997; Hagiwara et al. 1997). All of the megamaser galaxies show evidence for nuclear activity, being classified as either Seyfert 2 or LINER, and so there appears to be a link between the megamaser phenomenon and AGN activity. However, no megamasers have been detected in Seyfert 1 galaxies (Braatz, Wilson, & Henkel 1997). This suggests that either Seyfert 1s do not possess enough molecular gas with the physical conditions appropriate to produce 1.3 cm H_2O masers or the masers are beamed away from Earth.

There is strong evidence that H_2O megamasers are associated with the dense molecular gas located at the centers of galaxies. Interferometric studies show that the maser emission originates within about 1 pc or less of the nucleus (Claussen & Lo 1996; Miyoshi et al. 1995; Claussen et al. 1986). In particular, observations of maser emission from gas rotating at high velocities near the center of the LINER galaxy NGC 4258 indicate the presence of a thin, nearly edge-on molecular disk having an inner radius 0.13 pc, an outer radius 0.25 pc, and a significant warp (Miyoshi et al. 1995). These observations supply perhaps the best direct evidence to date for a circumnuclear disk of accreting matter in an active galaxy, and imply the presence of a $3.6 \times 10^7 M_{\odot}$ black hole at the center of NGC 4258.

The nature of H_2O megamasers and their relation to AGNs are still not clear. It may be that megamasers are present in a large fraction of AGNs, but are detected only in those for which the nuclear disk (a ubiquitous feature in unified models) is viewed close to edge-on. Alternatively, megamasers may result from special geometrical and/or physical conditions. For example, in the H_2O maser-detected galaxy NGC 4258 there is a combination of a nuclear hard X-ray source and a thin, warped molecular disk. The hard X-ray source irradiates the warped disk and gives rise to a molecular layer at temperatures 400 – 1000 K within which the water abundance is large (Neufeld & Maloney 1995). According to Neufeld, Maloney & Conger (1994), the physical conditions within this layer give rise to collisionally pumped H_2O maser emission with a predicted luminosity of $10^{2\pm 0.5} L_{\odot}$ per pc^2 of illuminated area. Another possible geometry involves a nuclear hard X-ray source surrounded by a geometrically thick molecular torus, with the maser emission arising from the inner surface of the torus (e.g., Greenhill et al. 1996). Of course, other sources of energy (e.g., shock waves, cf. Maoz & McKee 1998) may also be significant in heating the molecular gas to temperatures at which collisional pumping is effective. Nevertheless, the likelihood that X-ray heating is important and the tendency for H_2O megamaser-detected galaxies to have high column densities to their nuclei (Braatz, Wilson & Henkel 1997) indicates that X-ray observations are crucial for understanding the water vapor megamaser phenomenon.

To address these questions, we have undertaken a study of megamaser galaxies with the Advanced Satellite for Cosmology and Astrophysics (*ASCA*; Tanaka, Inoue & Holt 1994). Here we present results for the bright nuclear LINER NGC 1052 ($z = 0.0049$, $D = 19.6$ Mpc for $H_0 = 75$ km s $^{-1}$ Mpc $^{-1}$; $D = 29.4$ Mpc for $H_0 = 50$ km s $^{-1}$ Mpc $^{-1}$) which has $L_{maser} \simeq 200L_{\odot}$ (Braatz, Wilson & Henkel 1994). NGC 1052 is one of seven megamaser galaxies classified as LINERs and one of only two that are ellipticals. The spectral profiles of the masers in elliptical galaxies differ from the features found in other active nuclei. The emission lines are broad with ~ 90 km s $^{-1}$ FWHM and are not resolved into narrow components. VLBI observations of NGC 1052 show that the masers are not located in a disk around the central engine as in NGC 4258, but rather lie along the direction of the radio jet (Claussen et al. 1998). NGC 1052 was detected with the *Rosat* PSPC with a 0.1 – 2.0 keV flux of $\sim 6 \times 10^{-13}$ ergs cm $^{-2}$ s $^{-1}$ (Brinkmann, Siebert & Boller 1994). The *ASCA* observation is the first in the 2 – 10 keV band.

2. Observations and Analysis

NGC 1052 was observed with *ASCA* on 11 August 1996. *ASCA* contains four imaging telescopes that focus X-rays onto two pairs of detectors located at the focal plane. The detectors are the solid state imaging spectrometers (SIS; two detectors labeled S0 and S1) and the gas imaging spectrometers (GIS; two detectors labeled G2 and G3). The SIS data were obtained in 1-CCD readout mode, in which one CCD chip was exposed on each SIS, and were converted from FAINT to BRIGHT telemetry mode for analysis. The GIS data were obtained in standard pulse-height mode.

To produce good time intervals, the *ASCA* data were screened according to the following criteria. For all detectors, data collected during the satellite’s passage through the South Atlantic Anomaly (SAA) were discarded, as were data collected when satellite elevation angles were $\leq 5^{\circ}$. For the SIS, additional data were discarded when the geomagnetic cut-off rigidity (COR) was ≤ 6 GeV c $^{-1}$, when elevation angles during times of bright Earth were $\leq 20^{\circ}$, for times ≤ 16 s after an SAA passage, and for times ≤ 16 s after a transition from satellite day to satellite night. A prominent spike that remained in the SIS background after screening was removed, hot and flickering pixels were removed, and grade 0,2,3 and 4 photon events were selected. For the GIS, rise-time rejection was applied to exclude particle events, data were discarded for $COR \leq 4$ GeV c $^{-1}$, and times of soft and hard background flares were rejected (as described in the *ASCA* Data Reduction Guide 1997). After screening, 37.2 ks of good data were collected from each GIS and 37.6 and 36.2 ks of good data were collected from S0 and S1, respectively.

Spectra were extracted from each detector and grouped to have at least 20 counts per bin to allow the use of χ^2 statistics. Background was obtained from source-free regions in the same field. Our results do not change when using background from the standard blank-sky fields. The background-subtracted count rates for NGC 1052 range from 0.040 to 0.049 counts s^{-1} per detector, with the background accounting for 20% and 30% of the total rate in the SIS and GIS, respectively. Detector response matrices were generated with version 4.0 of the FTOOLS software. The four spectra were fitted together with version 10.0 of the XSPEC spectral fitting package (Shafer, Haberl & Arnaud 1989) and the model normalizations for each dataset were allowed to vary independently.

The *Rosat* PSPC observed NGC 1052 on 23 July 1993 for approximately 14 ks. The galaxy was also observed for a total of about 25 ks with the HRI, but since we focus on the spectrum, we do not include the HRI data in our analysis (see Guainazzi and Antonelli 1998). The PSPC spectrum was extracted from a circular region in the source field of about 1.2 arcmin radius. Background was taken from source-free positions located about 4 arcmin away from and surrounding the galaxy. Subtracting background yields a PSPC source count rate of 0.035 counts s^{-1} .

3. Results of Spectral Fitting

The observed 0.1 – 2.0, 0.6 – 2.0 and 2 – 10 keV luminosities of NGC 1052 are $\sim 4 \times 10^{40}$ ergs s^{-1} , $\sim 3.4 \times 10^{40}$ ergs s^{-1} , and $\sim 4 \times 10^{41}$ ergs s^{-1} , respectively (all luminosities are quoted for $H_0 = 50 \text{ km s}^{-1} \text{ Mpc}^{-1}$). Figure 1 shows the background-subtracted *ASCA* spectrum. The spectrum has been adapted for illustration purposes to have the best possible ratio of signal to noise at all energies. The data were averaged according to detector type, coarsely binned, and then plotted in the energy band for which that detector type has superior efficiency: the SIS below 5 keV and the GIS above 5 keV. Instrumental effects have not been removed, but can be estimated from the plotted telescope-plus-detector effective area curve.

The complex shape and hardness of the spectrum rules out a thermal bremsstrahlung or an ionized thermal plasma origin for the X-ray emission. Applying such models to the *ASCA* plus PSPC data yields extremely poor fits ($\chi^2/\nu = 2.8$) and implies unphysically high temperatures of $kT > 100 \text{ keV}$. Restricting the fits to energies less than 2.0 keV yields a temperature of $kT > 3 \text{ keV}$, which is consistent with that measured by Davis and White (1996) and is much higher than the temperatures of other elliptical galaxies with velocity dispersions similar to that of NGC 1052. In fact, Davis and White (1996) discard NGC 1052 from their statistical analysis of X-ray properties of elliptical galaxies based on the

argument that the soft X-ray flux is dominated by X-ray binaries or an AGN. Evidence for extended emission in the HRI (Guainazzi & Antonelli 1999) indicates some contribution from the galaxy which we investigate in §3.4.

3.1. Simple AGN Models

The hardness of the spectrum between 2 and 10 keV and the visible Fe K α fluorescence line at 6.4 keV verify the assertion made by Davis & White (1996) that the X-ray spectrum of NGC 1052 is dominated by something other than diffuse X-ray emitting gas, most likely an AGN. We favor this idea as opposed to a ‘normal’ ensemble of X-ray binaries for the following reason. The observed correlation between hard X-ray luminosity (L_X) and absolute blue-band (L_B) luminosity for early-type galaxies (Matsumoto, et al. 1997; Matsushita et al. 1994) predicts that X-ray binaries should contribute $\lesssim 10^{40}$ ergs s $^{-1}$ for NGC 1052 ($\log L_B/L_\odot = 10.2$); however this represents $\lesssim 2\%$ of the observed hard X-ray luminosity.

Unobscured AGN have approximately power-law X-ray spectra in the *ASCA* band and so we make the simplifying assumption that the *intrinsic* 0.6 – 10.0 keV spectrum has a power-law shape. We first consider simple AGN continuum models of the following form: (1) a power law with uniform, neutral absorption, (2) a power law that is partially covered by a patchy, neutral absorber, and (3) a uniformly absorbed power law plus flux scattered by an ionized electron scattering medium (a warm “mirror”). A Gaussian function is added, where appropriate, to model the Fe K α line. We list the best-fitting continuum and line parameters in Tables 1 and 2, respectively. A model that consists of a power law absorbed by the Galactic column density of $N_H = 3 \times 10^{20}$ cm $^{-2}$ (Table 1, model 1) provides a formally unacceptable fit ($\chi^2/\nu = 1.58$ for 325 d.o.f.) and yields an unusually small photon index of $\Gamma = 0.24$. The data divided by this model are shown in Figure 2a. Such a flat power law does a good job of approximating the data between 1 and 4 keV, but the data fall systematically above and below the model at energies < 1 keV and > 7 keV, respectively. The model does not include the Fe K α line, which is apparent in the data near 6.4 keV.

The simple power-law continuum model especially fails to explain the soft X-ray spectrum and so we investigate ways to model the extra flux below 1 keV (the “soft excess”). Our preliminary fits with pure thermal models (§3) allow us to rule out an origin of the soft X-rays entirely in a shock-heated plasma such as a galactic wind, with expected temperature of a few tenths of keV, or in a photo-ionized plasma, such as the warm electron scattering mirror, with expected temperature of ~ 0.9 keV, as seen in NGC 1068 (e.g., Marshall et al. 1993). Non-thermal models provide more reasonable results. The soft excess

can be described by leakage of nuclear continuum photons through a patchy absorber (model 2) or as scattered nuclear X-rays (model 3), but both models still imply a photon index of $\Gamma \sim 1.3$, which is smaller than the “canonical” value for Seyfert galaxies of ~ 1.7 to ~ 1.9 (Turner & Pounds 1989; Nandra & Pounds 1994). For the scattering interpretation, the scattered fraction is $\sim 22\%$, which is much higher than typical values of $\sim 1 - 2\%$ for Seyfert 2 galaxies (e.g., Mulchaey et al. 1993), although this problem is not as severe for more complex models (§§3.2 – 3.4).

To model the Fe $K\alpha$ line, we add an unresolved Gaussian to the power-law plus scattered flux model, which improves χ^2 by 20 (model 3_G). This represents a significant improvement in the fit ($>> 99\%$ confidence for the addition of two free parameters); however, even with such a large improvement, positive residuals are seen in all detectors at up to the 30% level near 0.6 and 2 keV (Figure 2b). Adding a second Gaussian to model the curvature in the spectrum between 4 and 8 keV allows the photon to increase and N_{H} to decrease, which in turn results in a better fit to the soft excess and ~ 2 keV bump and thus improves the fit further (model 3_{2G}). The problem with this model is that the line width increases dramatically to the implausible value of $\sigma = 2.4$ keV. This excellent *empirical* fit indicates more complexity in the spectrum than the superposition of a single-absorbed power law and soft X-ray component. Below we investigate the likely possibilities.

3.2. A Dual-Absorber Model

Since the flatness of the spectrum between 1.5 and 6 keV (Figure 1, 2a,b) cannot be described by simple power-law models (models 1 through 3_G, Table 1), we investigate physical models that can produce a flat, observed spectrum but allow the intrinsic spectrum to be steeper and more similar to that expected for an AGN. One possibility is that the spectrum is modified by a complex absorption structure. We therefore tried a continuum model that consists of an intrinsically power-law nuclear spectrum of which a fraction C is attenuated by a column density N_{H1} , a fraction $1 - C$ is attenuated by a column density N_{H2} , and a fraction is scattered into our line of sight (the soft excess), plus a single Gaussian representation of Fe $K\alpha$. This so-called “dual absorber” model (model 4) is more physically reasonable than the double-Gaussian model (3_{2G}) and can explain the unusually flat X-ray spectra of other heavily absorbed AGN such as NGC 4151 (Weaver et al. 1994) and NGC 5252 (Cappi et al. 1996). The corresponding physical scenario might be an extended X-ray source, such as an accretion disk corona, covered by a clumpy or layered absorber.

The dual-absorber model describes the data as well as the empirical double-Gaussian model. The ratio of power-law normalizations at 1 keV for the scattered component

(1.5×10^{-4} photons $\text{keV}^{-1} \text{cm}^{-2} \text{s}^{-1}$) and the heavily absorbed component (13×10^{-4} photons $\text{keV}^{-1} \text{cm}^{-2} \text{s}^{-1}$) yields a scattered fraction of $\sim 11\%$. To fully reproduce the spectrum we require 70% of the intrinsic flux to be absorbed by a large column of $N_{\text{H1}} = 3 \times 10^{23} \text{cm}^{-2}$ and 30% to be absorbed by a smaller column of $N_{\text{H2}} = 5 \times 10^{22} \text{cm}^{-2}$. For this model, the absorption-corrected 2 – 10 keV flux is $8 \times 10^{-12} \text{ergs cm}^{-2} \text{s}^{-1}$, yielding an intrinsic 2 – 10 keV luminosity of $8 \times 10^{41} \text{ergs s}^{-1}$.

3.3. Models That Include Compton Reflection

Another way to produce a flat, hard spectrum (with photon index comparable to the observed value of $\Gamma = 0.16$ above 1 keV) is by Compton reflection from a dense, neutral medium (Lightman & White 1988; Guilbert & Rees 1988). We include a reflection component in the next set of models by means of the *hrefl* model in XSPEC. This model uses an elastic scattering approximation that is valid up to energies of 15 keV and predicts the reflected spectrum from a cold, optically thick disk illuminated by a point source located at height H above the center of the disk. The reflected component suffers heavy photoelectric absorption, and the model is the sum of X-rays from the directly-viewed point source and those reflected from the disk. The model parameters that can be varied are the height of the point source above the disk (here taken to be small compared to the disk radius), the abundance (Z) of the gas in the disk, the inclination (θ) of the disk normal with respect to the observer’s line of sight, the fraction (f_i) of the spectrum of the point source (here taken to be a power law with index Γ) that the observer sees directly, and a measure (R) of the relative amount of reflected flux, which is normalized to unity when the point source emits isotropically and the disk covers 2π steradians as seen from the point source. If the photon spectrum of the point source is $N(E)$ and the reflected continuum from the disk in our direction is $R(E)$ (both in photons $\text{cm}^{-2} \text{s}^{-1} \text{keV}^{-1}$), then the model spectrum for a given inclination and abundance is $M(E) = f_i \times N(E) + R \times R(E)$. If H is \ll the radius of the disk, the point source emits isotropically, is time stable, and is not blocked from our view, then $f_i = 1$ and $R = 1$. If, on the other hand, we see none of the X-rays from the point source, then $f_i = 0$.

Care must be taken when interpreting the reflection model. The shape of the model X-ray spectrum is a function of f_i , Γ , and $R \times R(E)$, the last being also a function of Z , θ and the solid angle subtended by the disk at the point source. Comparison with the observed spectrum can provide the relative amounts of directly viewed and reflected emission, but interpretation in terms of these parameters is ambiguous. For example, a relatively large amount of reflected flux can indicate a large covering factor for the disk or a

small f_i . The *ASCA* data cannot determine Γ or θ , so we fix Γ at its canonical observed value for AGN of 1.7 (Turner & Pounds 1989), and we arbitrarily fix θ at 60° .

If the spectrum above 2 keV represented a directly-viewed nuclear source plus reflection with the canonical parameters $R = 1$ and $f_i = 1$, we would expect the nuclear source to dominate up to ~ 8 keV and then the spectrum would flatten. Since the observed spectrum remains flat down to almost 1 keV, we can immediately rule out this possibility. If we instead assume that almost all X-rays above 2 keV are reflected (the flattening being due to photoelectric absorption), then the fit is acceptable (Table 1, model 5) and we find $f_i = 0.007 \pm 0.002$ for $R = 1$. The small f_i implies that the central source is either highly anisotropic, highly time-variable, or is hidden behind gas with a large column density. While the first two possibilities cannot be excluded, we feel that the most plausible explanation for the small amount of flux seen directly is that the power-law source is blocked from our view. Assuming full coverage of the nuclear X-ray source, we find that the nuclear absorbing column must be greater than $3 \times 10^{23} \text{ cm}^{-2}$ to attenuate the nuclear flux so that reflection dominates the spectrum.

One problem for the reflection model is the ~ 40 eV equivalent width (EW) of the Fe $K\alpha$ line, which is much smaller than expected for a purely reflected spectrum. Fully blocked Seyfert 2 galaxies like Mkn 3 (Iwasawa et al. 1994), NGC 4945 (Done, Madejski, & Smith 1996), and Circinus (Matt et al. 1996) have Fe $K\alpha$ EWs of $\sim 1 - 2$ keV. To account for the weak Fe $K\alpha$ line within the context of the reflection model, the iron abundance must be $\leq 0.05Z_\odot$, which is implausibly small. On the other hand, the lower column densities implied by the dual-absorber model (10^{22} to a few times 10^{23} cm^{-2}) allow a scenario in which we view the nuclear source directly above ~ 5 keV. In this case, an Fe $K\alpha$ line with an EW of ~ 200 eV could be produced in a Compton-thick disk or in a spherical distribution of clouds with a large covering factor. Since the properties of the Fe $K\alpha$ line are much more consistent with transmission than reflection models, we argue in favor of the dual-absorber interpretation.

We have also searched for line emission in addition to Fe $K\alpha$. Reflection-dominated Seyfert 2 galaxies possess fluorescence emission lines due to elements such as Mg, Si, and S (e.g., Reynolds et al. 1994). We derive upper limits of $\text{EW} \sim 200$ eV for such features.

3.4. Models That Include Thermal Emission

We also examine descriptions of the soft excess that include a Mewe-Kaastra (“Mekal”) plasma model with solar abundances. Describing the soft emission as purely thermal

provides an acceptable fit for both the dual-absorber and reflection models (models 6 and 7). However, the best fit includes thermal and scattered emission (model 8). In this case, $\sim 15\%$ of the soft excess is thermal with a temperature of $kT = 0.53_{-0.26}^{+0.34}$ keV, a 0.1 – 2 keV flux of $5.8_{-2.3}^{+2.5} \times 10^{-14}$ ergs cm^{-2} s^{-1} , and a 0.1 – 2 luminosity of $5.9_{-2.4}^{+2.5} \times 10^{39}$ ergs s^{-1} . The properties of the thermal component are consistent with those of other elliptical galaxies with velocity dispersions similar to NGC 1052 (Davis & White 1996). This result, combined with the extended nature the soft X-ray emission in the HRI (Guainazzi & Antonelli 1999), suggests that the thermal component originates in the hot interstellar medium of the elliptical galaxy.

The thermal component we measure can account for only 20% of the observed luminosity in the HRI extent quoted by Guainazzi and Antonelli (1999). However, there are many uncertainties in both measurements. For example, the HRI data quality make is difficult to determine exactly what fraction of the source is extended. Also, the HRI and PSPC have different sensitivities at 0.5 keV and so a direct comparison would have to take this into account. In our best-fit model that includes scattered and thermal emission, the scattered fraction is higher than expected ($\sim 11\%$), which suggests we may be underestimating the thermal contribution and overestimating the scattering contribution. One way this could happen is if we have the abundances wrong. Better data are needed to resolve this issue.

3.5. Summary of Spectral Fitting Results

We have shown that the nuclear source in NGC 1052 is heavily absorbed by gas having a column density of $\geq 10^{23}$ cm^{-2} . Compton reflection models imply that we see less than 5% of the intrinsic source directly, while dual-absorber models require $\sim 70\%$ of the source to be absorbed by a column of $N_{\text{H}} = 3 \times 10^{23}$ cm^{-2} and $\sim 30\%$ to be absorbed by a column of $N_{\text{H}} = 3 - 5 \times 10^{22}$ cm^{-2} . The weakness of the Fe $K\alpha$ line compared to that predicted if the X-rays are reflected argues in favor of a complex absorption structure (represented by the dual absorption model). The prominent soft excess can be described as nuclear flux scattered by ionized gas or as partial covering of the nuclear source, plus a 15% contribution from a ~ 0.5 keV thermal component, which most likely arises from the galaxy.

4. Discussion

As already mentioned, the observed 2 – 10 keV luminosity of NGC 1052 is $\sim 4 \times 10^{41}$ ergs s^{-1} . Our most plausible physical models imply absorption-corrected luminosities of ~ 2 to 50 times this value for the dual-absorber and reflection models, respectively. Both of these models require gaseous columns of $N_H \gtrsim 3 \times 10^{23}$ cm^{-2} . Such large absorbing columns are entirely consistent with X-ray observations of other megamaser galaxies. For example, NGC 1068 (Iwasawa et al. 1997), NGC 4945 (Done, Madejski & Smith 1996), and Circinus (Matt et al. 1996) are completely blocked in the 2 – 10 keV band.

We can compare the density of the gas inferred from the maser observations with the column density inferred from the X-rays. The size of the maser spots in NGC 1052 is estimated to be $\leq 10^{17}$ cm (Claussen et al. 1998). The gas should maser most efficiently at a density a bit below the quenching density. Thus a reasonable estimate for the density would be $10^8 - 10^{10}$ cm^{-3} , which predicts a column density less than $10^{25} - 10^{27}$ cm^{-2} . This upper limit is entirely consistent with the inferred X-ray column of $> 3 \times 10^{23}$ cm^{-2} .

The relationship between the X-ray absorber and the masing gas in NGC 1052 is different from the most well-studied megamaser galaxy, NGC 4258. In NGC 4258, the masers and the absorption originate in an approximately Keplerian accretion disk that orbits the central source. In NGC 1052, the VLBA map shows the maser spots to be at a projected distance of ~ 0.04 pc from the believed nucleus (Claussen et al. 1998), and they lie along the direction of the radio jet. The maser emissions are only seen from those molecular clouds being hit by or located in front of the radio jet. For example, the masing clouds could be located in the accretion disk between us and the jet if the SW radio jet (with which the masers coincide) is the one pointed away from Earth. Conversely, the X-ray absorption arises from gas along our line of sight to the nucleus proper. If the nuclear X-ray source is coincident with the radio nucleus inferred from 43 GHz observations (Vermeulen et al. 1998), the observed masing clouds (Claussen et al. 1998) must be spatially separate from those that absorb the X-ray emission, although the latter might also be part of the accretion disk.

The absence of a strong Fe $K\alpha$ fluorescence line with an equivalent width of 1 – 2 keV argues against a purely reflected X-ray spectrum, and also seems to fit the pattern seen in other LINERS by e.g., Terashima et al. (1997). This may mean that there is no optically-thick inner accretion disk around the nuclei of these objects. An attractive explanation is that the inner disks are actually ion tori (i.e., advection-dominated disks) as proposed originally by Chen & Halpern (1989). More high-sensitivity X-ray observations of masing galaxies are needed to provide reliable evidence for or against advection-dominated accretion disks.

5. Conclusions

The observed X-ray spectrum of the LINER galaxy NGC 1052 is unusually flat, $\Gamma \sim 0.2$, between the energies of 1.5 and 6 keV. This is a signature of significant absorption which modifies the intrinsic spectrum. The nuclear X-ray emission either traverses a complex distribution of absorbing material with column densities of up to a few $\times 10^{23}$ cm^{-2} , or is Compton reflected from gas with a column $\gtrsim 10^{24}$ cm^{-2} ; however, the moderate Fe K α EW of ~ 270 eV favors the complex-absorber model as the more likely physical scenario. The inferred 2 – 10 keV intrinsic (absorption-corrected) luminosity is $\sim 8 \times 10^{41}$ or $\sim 2 \times 10^{43}$ ergs s^{-1} for the complex absorber and Compton-reflection models, respectively. The large column densities are consistent with the presence of luminous water vapor masers in NGC 1052; however, the absorbing gas appears to be spatially separate from the masing gas in this galaxy.

This research has made use of the HEASARC database. KAW acknowledges support from NASA long-term space astrophysics grant NAG 53504. CAH acknowledges support from NATO grant SA.5-2-05 (GRG.960086). ASW thanks NASA and NSF for support under grants NAG 81027, NAG 53393, and AST 9527289.

REFERENCES

- Braatz, J. A., Wilson, A. S. & Henkel, C. 1994, ApJ, 437, L99
- Braatz, J. A., Wilson, A. S. & Henkel, C. 1996, ApJS, 106, 51
- Braatz, J. A., Wilson, A. S. & Henkel, C. 1997, ApJS, 110, 321
- Brinkmann, W., Siebert, J. & Boller, Th. 1994, A&A, 281, 355
- Cappi, M., Mihara, T., Matsuoka, M., Brinkmann, W., Prieto, M. A. & Palumbo, G. G. C. 1996, ApJ, 456, 141
- Chen, K. & Halpern, J. P. 1989, ApJ, 344, 115
- Claussen, M. J. & Lo, K.-Y. 1986, ApJ, 308, 592
- Claussen, M. J., Diamond, P. J., Braatz, J. A., Wilson, A. S. & Henkel, C. 1998, ApJ, 500, 129
- Davis, D. S. & White, R. E. 1996, ApJ, 470, L35
- Done, C., Madejski, G. M. & Smith, D. A. 1996, ApJ, 463, L63

- Greenhill, L. J., Gwinn, C. R., Antonucci, R. & Barvainis, R. 1996, *ApJ*, 472, L21
- Greenhill, L. J., Herrnstein, J. R., Moran, J. M., Menten, K. M. & Velusamy, T. 1997, *ApJ*, 486, L15
- Guainazzi, M. & Antonelli, L. A. 1998 (astro-ph/9812385)
- Guilbert, P. W. & Rees, M. J. 1988, *MNRAS*, 233, 475
- Hagiwara et al. 1997, *PASJ*, 49, 171
- Iwasawa, K., Fabian, A. C. & Matt, G. 1997, *MNRAS*, 289, 443
- Iwasawa, K., Yaqoob, T., Awaki, H. & Ogasaka, Y. 1994, *PASJ*, 46, L167
- Lightman, A. P. & White, T. R. 1988, *ApJ*, 335, 57
- Maoz, E. & McKee, C. F. 1998, *ApJ*, 494, 218
- Marshall, F. et al. 1993, *ApJ*, 405, 168
- Matsumoto, H., Koyama, K., Awaki, H., Tsuru, L., Loewenstein, M. & Matsushita, M. 1997, *ApJ*, 482, 133
- Matsushita, K. et al. 1994, *ApJ*, 436, L41
- Matt, G. et al. 1996, *MNRAS*, 281, L69
- Miyoshi, M., Moran, J., Herrnstein, J., Greenhill, L., Nakai, N., Diamond, P. & Inoue, M. 1995, *Nature*, 373, 127
- Mulchaey, J. S., Colbert, E., Wilson, A. S., Mushotzky, R. F. & Weaver, K. A. 1993, *ApJ*, 414, 144
- Nandra, K. & Pounds, K. 1994, *MNRAS*, 268, 405
- Neufeld, D. A., Maloney, P. R. & Conger 1994, *ApJ*, 436, L127
- Neufeld, D. A., & Maloney, P. R. 1995, *ApJ*, 447, L17
- Reynolds, C. S., Fabian, A. C., Makishima, K., Fukazawa, Y. & Tamura, T. 1994, *MNRAS*, 268, L55
- Shafer, R. A., Haberl, F. & Arnaud, K. A. 1989, “XSPEC: An X-ray Spectral Fitting Package” (ESA TM-09; Paris: ESA)

- Tanaka, Y., Inoue, H. & Holt, S. S. 1994, PASJ, 46, L37
- Terashima, Y., Kunieda, H., Serlemitsos, P. J. & Ptak, A. 1997, IAU Symposium 188, "The Hot Universe" (Japan), in press
- Turner, T. J. & Pounds, K. A. 1989, MNRAS, 240, 833
- Vermeulen, R., Kellermann, K. & Zensus, A. 1998, in ASP Conf. Ser. 144, Radio Emission from Galactic and Extragalactic Compact Sources, IAU Colloq. 164, ed. J. A. Zensus, J. M. Wrobel & G. B. Taylor (San Francisco: ASP), in press
- Weaver, K. A., Yaqoob, T., Holt, S. S., Mushotzky, R. F., Matsuoka, M. & Yamauchi, M. 1994, ApJ, 436, L27

Table 1. *ASCA* + PSPC Spectral Results^a

Model	N_H^b [$\times 10^{22}$]	f_c^c or kT^d	Γ_{int}^e	$A_{\Gamma_{int}}^f$ [$\times 10^{-4}$]	$A_{\Gamma_{scatt}}^g$ [$\times 10^{-4}$]	f_i^h or A_{MEKAL}^i	χ^2/dof^j
1	0.03(f)	...	0.24 ± 0.05	$0.95^{+0.07}_{-0.06}$	512.2/325
2	$11.5^{+3.3}_{-2.6}$	$0.80^{+0.07}_{-0.10}$	1.26 ± 0.12	8.3 ± 1.5	354.4/323
3	$12.8^{+2.9}_{-2.5}$...	1.28 ± 0.15	6.8 ± 1.0	1.50 ± 0.09	...	354.6/322
3 _G	$11.6^{+3.5}_{-2.7}$...	1.31 ± 0.18	6.7 ± 1.6	1.5 ± 0.08	...	334.2/322
3 _{2G}	$4.5^{+5.7}_{-2.7}$...	$1.58^{+0.30}_{-0.28}$	$2.9^{+1.6}_{-1.1}$	1.5 ± 0.1	...	315.1/318
4	$4.9^{+2.0}_{-1.4}$...	$1.65^{+0.37}_{-0.25}$	$4.5^{+1.7}_{-1.6}$	1.5 ± 0.14	...	314.4/320
	$30.0^{+16.8}_{-11.6}$			$13.0^{+4.5}_{-3.4}$			
5	0.03(f)	...	1.7(f)	173 ± 10	...	0.007 ± 0.002	341.9/324
6	0.03(f)	$0.53^{+0.34}_{-0.26}$	1.7(f)	180 ± 15	0.18 ± 0.09	0.006 ± 0.002	327.8/322
7	$0.88^{+0.32}_{-0.34}$	0.53(f)	1.7(f)	3.2 ± 0.5	...	0.61 ± 0.08	321.9/320
	$18.6^{+5.2}_{-4.1}$			$15.9^{+2.1}_{-1.8}$			
8	$3.05^{+1.48}_{-1.20}$	0.53(f)	1.7(f)	$4.0^{+1.6}_{-1.5}$	1.1 ± 0.6	0.25 ± 0.09	301.1/320
	$25.8^{+17.5}_{-11.0}$			$9.7^{+6.1}_{-4.7}$			

Notes to Table 1:

^aModels are (1) uniformly-absorbed power law, (2) partially covered power law, (3) absorbed power law plus scattered flux, (4) dual absorber plus scattered flux, (5) Compton reflection, (6) Compton reflection plus MEKAL plasma, (7) dual absorber plus MEKAL plasma, (8) dual absorber plus scattered flux and MEKAL plasma. All models include Galactic absorption with $N_{\text{H}} = 3 \times 10^{20} \text{ cm}^{-2}$. For reflection models, $\theta = 60^\circ$ and $\Omega = 2\pi$. The photon index of the scattered component (Γ_{scatt}) is assumed equal to the intrinsic photon index (Γ_{int}). Models 3_G through 6 include an Fe K α line; Model 3_{2G} contains an additional Gaussian (Table 2). A fixed parameter is denoted by (f). Errors on normalization are 90% confidence for 1 free parameter ($\chi^2 + 2.7$). Other errors are 90% confidence for 2 (models 1, 3, 4), 3 (models 2, 3_G, 5, 6, 7) or 4 (model 3_{2G}, 8) parameters, which is $\chi^2 + 4.6$, $\chi^2 + 6.4$, or $\chi^2 + 7.1$, respectively.

^bColumn density in units of cm^{-2} .

^cFraction of the X-ray source covered by absorbing gas.

^dMEKAL plasma temperature in keV.

^eThe intrinsic photon index.

^fNormalization of the intrinsic power law in units of photons $\text{keV}^{-1} \text{ cm}^{-2} \text{ s}^{-1}$ at 1 keV.

^gNormalization of the scattered power law in units of photons $\text{keV}^{-1} \text{ cm}^{-2} \text{ s}^{-1}$ at 1 keV.

^hFraction of intrinsic nuclear flux that is seen directly.

ⁱ Normalization of MEKAL plasma in units of photons $\text{keV}^{-1} \text{ cm}^{-2} \text{ s}^{-1}$ at 1 keV.

^jd.o.f.=degrees of freedom, which is the number of data points minus the number of free parameters.

Table 2. Spectral Results: Parameters of the Fe K α line^a

Model	E ₁ ^b [keV]	σ_1^c [keV]	Norm ₁ ^d [$\times 10^{-5}$]	EW ₁ ^e [eV]	E ₂ ^b [keV]	σ_2^c [keV]	Norm ₂ ^d [$\times 10^{-5}$]	EW ₂ ^e [keV]
3 _G	6.36 ^{+0.23} _{-0.16}	0.02(f)	1.78 \pm 1.04	302 \pm 190
3 _{2G}	6.37(f)	0.02(f)	1.25 \pm 0.56	200 \pm 170	5.5 ^{+1.2} _{-4.0}	2.4 ^{+3.7} _{-1.6}	36 \pm 12	20 \pm 5
4	6.37(f)	0.02(f)	1.9 ^{+0.9} _{-0.8}	302 ⁺¹⁵⁰ ₋₁₄₀
5	6.37(f)	0.02(f)	0.4 ^{+0.5} _{-0.4}	46 ⁺⁵⁸ ₋₄₆
6	6.37(f)	0.02(f)	0.3 ^{+0.4} _{-0.3}	35 ⁺⁴⁶ ₋₃₅
7	6.37(f)	0.02(f)	1.8 \pm 0.7	267 \pm 100
8	6.37(f)	0.02(f)	1.8 \pm 0.8	270 \pm 120

^aModels are defined in Table 1. A fixed parameter is denoted by (f).

^bGaussian energy.

^cGaussian width.

^dGaussian line flux in units of photons cm⁻² s⁻¹.

^eGaussian equivalent width.

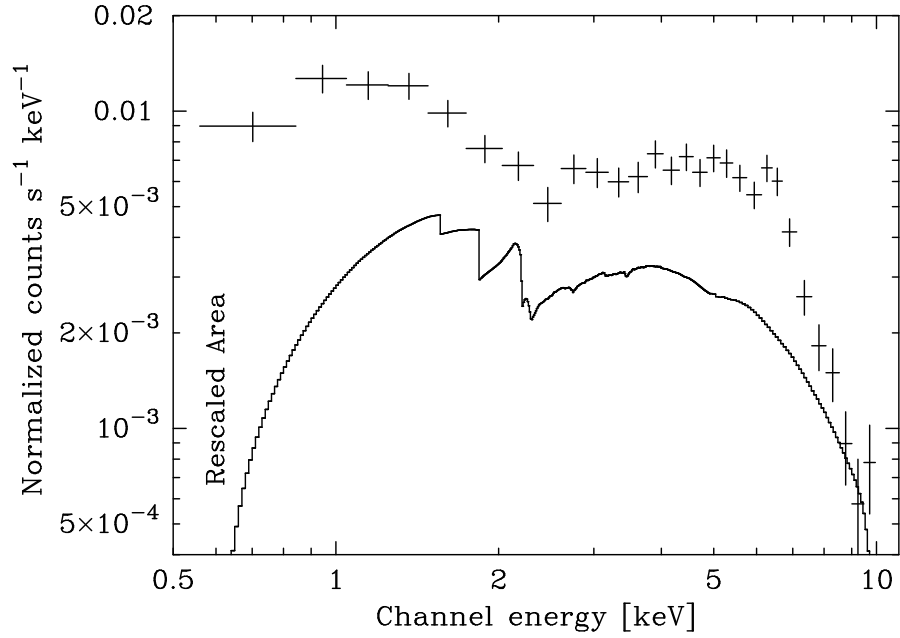


Fig. 1.— The *ASCA* spectrum of NGC 1052. The signal-to-noise ratio is maximized by coarsely binning the averaged data from each set of detectors and then plotting the SIS data below 5 keV and the GIS data above 5 keV. The solid line is the corresponding telescope-plus-detector effective area curve sampled at full spectral resolution and arbitrarily rescaled.

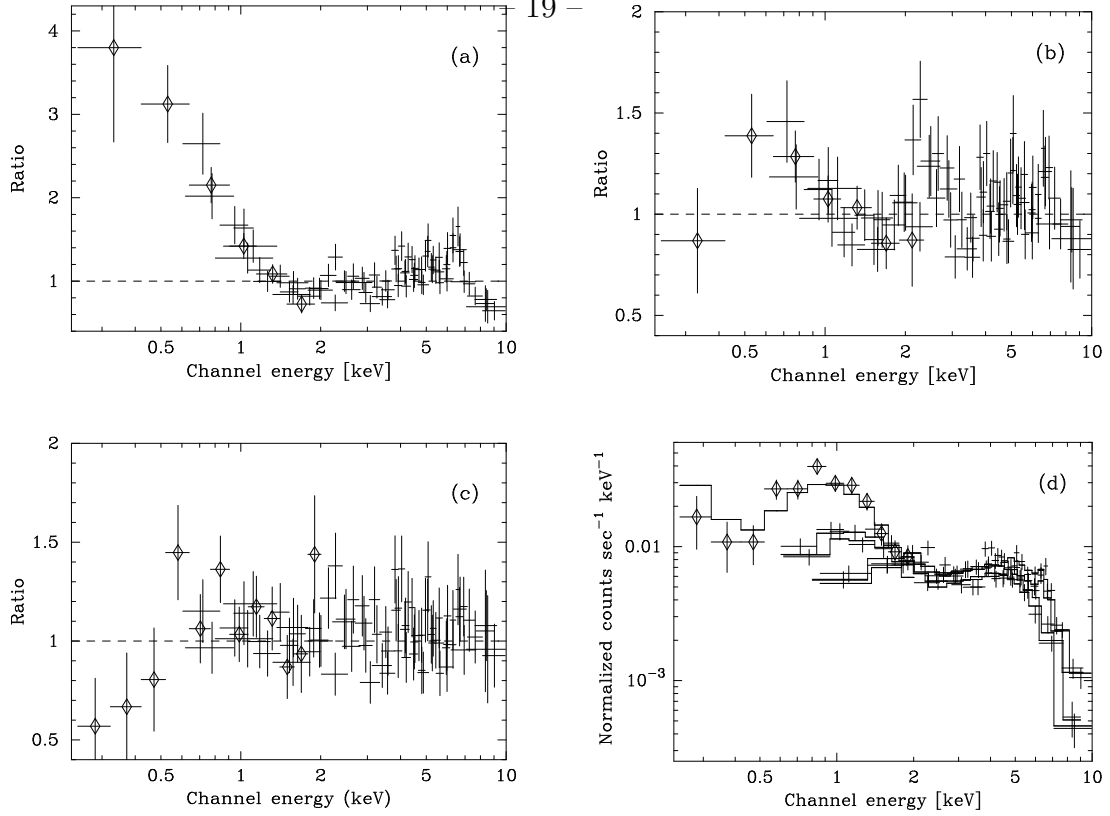


Fig. 2.— The *ASCA* SIS and GIS data (crosses) and *Rosat* PSPC data (diamonds). The first three panels show the ratio of the data to a model that consists of (a) a power law with Galactic absorption (Table 1, model 1); (b) an absorbed power law above ~ 2 keV, a scattered power law absorbed by only the Galactic column below ~ 2 keV and a narrow Gaussian at 6.37 keV (Table 1, model 3_G); (c) a dual absorber plus scattered flux model (Table 1, model 4). Panel (d) shows the observed spectrum and the dual-absorber plus scattered flux model (panel c) folded through the instrumental response. Data from all 5 instruments are coarsely binned and plotted separately. These diagrams illustrate the level of goodness of the statistics and so are not optimized for discrimination between the SIS and GIS data nor between observed and modeled data. The PSPC data in panels c and d are binned less coarsely than in panels a and b to better show the deviations near 0.5 keV caused by the lack of including a thermal component in model 4.

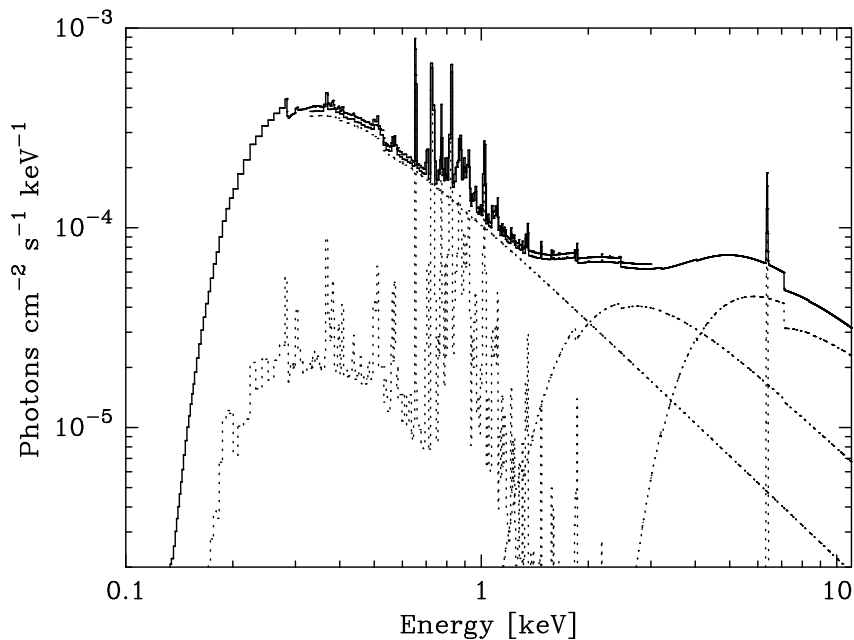


Fig. 3.— The model that best describes the $\sim 0.1 - 10.0$ keV spectrum of NGC 1052: a power-law continuum with 70% absorbed by $N_{\text{H1}} = 3 \times 10^{23} \text{ cm}^{-2}$ and 30% absorbed by $N_{\text{H2}} = 3 \times 10^{22} \text{ cm}^{-2}$, a soft X-ray component that consists of 85% scattered flux and 15% thermal plasma emission with $kT = 0.53$ keV, and an unresolved Fe $K\alpha$ line with $EW = 270$ eV.